05- SURFACE WATER MAPPING AND EXTRACTION METHODS USING REMOTE SENSING DATA: A COMPARATIVE STUDY IN VOJVODINA (NORTHERN SERBIA)

Marta Estanqueiro[1,2] and Sojan Mathew[3]

[1] *University College Dublin, School of Archaeology*
[2] *University of Coimbra, Research Centre of Archaeology, Arts and Heritage Sciences (CEAACP)*
[3] *University College Dublin, School of Geography*

Abstract
The increasing availability of open source, space borne multispectral (Sentinel-2) and radar data (Sentinel-1) with high spatial and temporal resolution, has revolutionized the way we monitor and quantify the spatio-temporal changes in surface waters. A multiplicity of remote sensing approaches have been proposed for surface water mapping. In this investigation, five different approaches were used to evaluate their relative performance, including spectral water indices and supervised classification algorithms. They were applied to a case study along the Tamis River in the Vojvodina region (Northern Serbia) in an area that included several artificial ponds. The results of each method were subsequently compared. Sentinel-2 multispectral imagery data were used to test the effectiveness of the normalized difference water index (NDWI) and Xu's modified NDWI (MNDWI), as well as to perform a maximum likelihood classification. The results of Sentinel-2 were compared with Sentinel-1 synthetic aperture radar data (SAR) using classification methodologies such as random forest (RF) classifier and an intensity threshold approaches to discriminate water from non-water features. Sentinel-2 results showed a higher performance of MNDWI in relation to NDWI, with a built-up noise reduction. Yet, the maximum likelihood supervised classification obtained the best results of all five methods, with an overall accuracy of 95% and a Kappa statistic of 0.89.

Sentinel-1 classification results were very similar to each other and obtained the same value in the overall accuracy and Kappa coefficient. Comparing the results with the ones obtained previously with the Sentinel-2 data, the SAR approaches correctly identified the water in the artificial ponds but showed difficulty in identifying the Tamis River. This outcome can be ascribed to the low intensity backscatter values from mixed pixels coupled with reduced width of the river across the study area. The results of this investigation provide an understanding of the uncertainties and error associated with the applications of Sentinel-2 and Sentinel-1 for flood plain monitoring and mapping as well as mitigation measures.

Key words: *remote sensing, multispectral, SAR, indices, classification, accuracy, streams, flood plain, mapping*

1. INTRODUCTION

Remote sensing represents a powerful tool to obtain information about the Earth's surface at a global and local scale, and the resulting datasets regarding the atmosphere, climate, land, vegetation, water, and pollution can now be easily accessed by users of various backgrounds. The information provided by remote sensors can help us to detect, identify, map, monitor and manage several natural resources with applications in diverse fields such as agriculture, geosciences, environmental management, weather forecasting, natural risk assessment, pollution control, etc. whose correct management is crucial for human life.

One of the applications of remote sensing techniques has been the mapping of surface water. The identification of inundated areas is also critical as flooding events are a major concern, resulting in both human and economic losses due to material damage and crop destruction. Correctly mapped/delineated flood areas allow us to build flood maps, monitoring and delimitating the

affected areas to send help fast and look for solutions to prevent or mitigate the consequences caused by these events.

To identify flooded areas, it is necessary to map surface water and distinguish permanent water bodies. Several methods have been developed, using remote sensing techniques such as optical (Sentinel-2) and active synthetic aperture radar (SAR) data (e.g., Sentinel-1). The first, takes advantage of water near-infrared (NIR) absorption, thus allowing the water to be distinguished from the land features. Yet, optical satellites are limited by weather conditions (cloud cover) and lack of sunlight. Representing a powerful alternative, the ones using radar data, do not have the constraints of atmospheric conditions and dependence of daylight using the backscatter values of microwaves emitted by the sensor to differentiate water bodies from the remaining features, such as vegetation and soil. Water is distinguished through its low backscatter values, due to the smooth surface which translates in specular reflection. Nevertheless, SAR data also have challenges and limitations in their use. The sensitivity to the characteristics of the land surface such as roughness, geometry or dielectric constant makes it more difficult to interpret them, than optical data, and to be able to correctly identify an object a minimum number of pixels is a requirement necessary to obtain a good result.

Between the most common methods to map surface water using optical and Synthetic Aperture Radar (SAR) data are supervised classifications, histograms threshold or binarization, and water indices, such as the Normalised Difference Water Index (NDWI) and the Modified Normalised Difference Water Index (MNDWI).

The aim of this investigation was to assess the relative accuracy of commonly used remote sensing techniques for mapping and extracting water bodies, while applying them to the Serbian Banat area, a region that had suffered several flooding events. This comparative study will examine some of the advantages and disadvantages of these methods when applied to alluvial plains, while the results can be transposed to other similar areas.

1.1.Study area

The Banat plains are a flat landscape located in the Carpathian Basin (south-eastern Europe) and home to the confluence of major river networks centred on the Danube. It includes part of Hungary, Romania, and northern Serbia. This work focuses on the Serbian part of Banat, located in its northeast (Fig.1). Geographically the study area is limited by the River Tisza in the west, the Danube in the south and the Romanian border in the east.

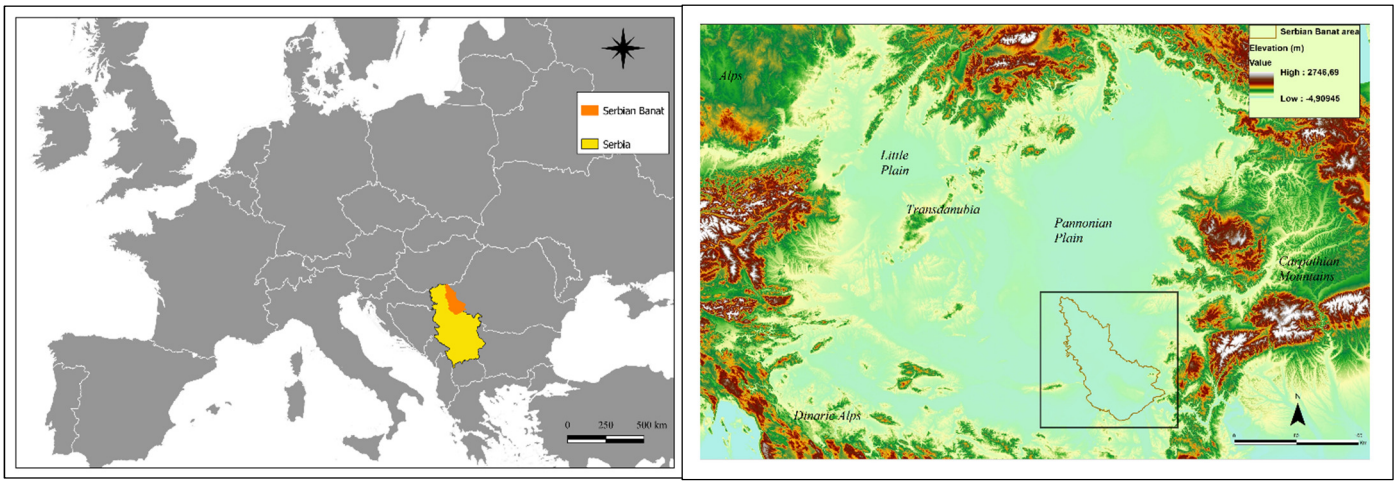

Figure 1: *Geographic location of the study area in Europe and Serbia (left) and Carpathian Region relief with study area highlighted (right)*

The Carpathian region is encircled by a mountain system formed by the Carpathian Mountains in the north and east, the Dinaric Alps in the south and the Alps in the west (Fig.1).

Inside the Carpathian Mountain Arc lies the depressed Carpathian Basin, composed by two major flat alluvial lowlands, the Little Plain and the Pannonian Plain separated by the central Transdanubia lower mountains and hills.

The study area is characterized by a very flat relief (100-200m a.m.s.l) with a low altitude mountain, Vršac Mountain (639m). It has a mild temperate climate with an average temperature of 21ºC – 23ºC in summer and cold and dry winters (Pavlović et al. 2017) (Fig.2).
The Dinaric mountains form an orogenic barrier to the west winds from the Adriatic coast, affecting the precipitation patterns in the Balkan Peninsula resulting in a low amount of precipitation in Serbia, especially in the north, with an annual average of 500- 600 mm. Precipitation is concentrated mostly in early summer and in smaller amounts in November and March (Malinović-Milićević et al. 2018).

The Serbian Banat hydrographic network belongs to the Middle Danube. Beside the Danube and its two main tributaries, Tisza and Tamis, other smaller watercourses exist. Many of these are torrent rivers and streams, overflowing in the spring with the snowmelt and in June with the heavy rainfall.
Despite massive engineering works, the low gradient of the alluvial plain and the meandering form of the watercourses lead to a slow flow and a potential risk of flooding.

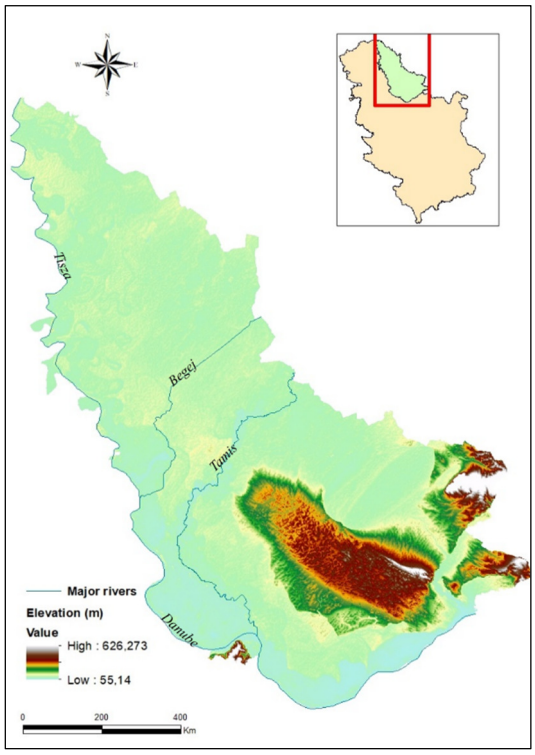

Figure 2: *Serbian Banat relief*

2. METHODOLOGY

2.1 Sentinel-2 data

The Sentinel-2 multispectral data are freely available and are gathered by the twin satellites, 2-A, and 2-B. The data have a spatial resolution of 10m in the bands 2, 3, 4 and 8, 20m in the 5, 6, 7, 8a, 11 and 12, and 60m in the bands 1,9 and 10.

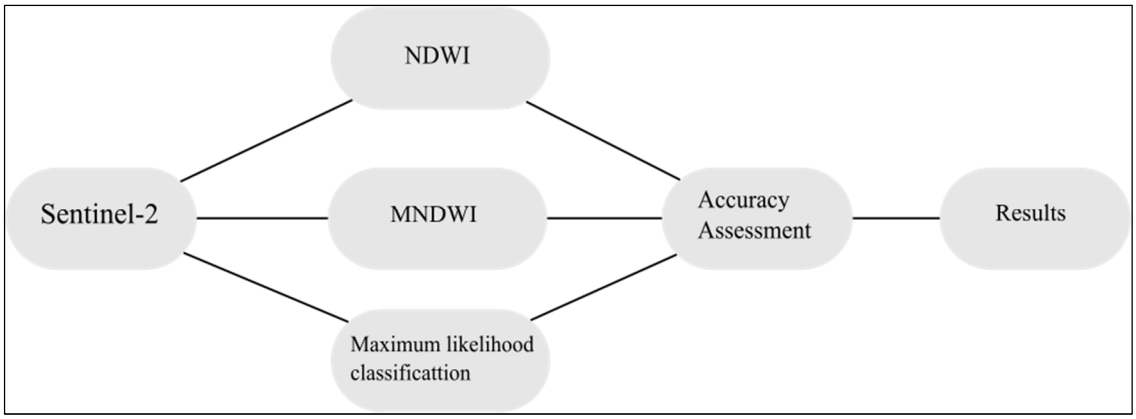

Figure 3: *Flowchart of methodological procedures for Sentinel-2 data.*

The work of both satellites allows a revisit time of 5 days, and the data are available to the public in 100km tile images. The level 1C products, used in this study, are pre-processed with radiometric, geometric correction and orthorectification and available in UTM/WGS84 projection. The data from Sentinel-2 were accessed through the Earth Explorer website from U.S Geological Survey (https://earthexplorer.usgs.gov/) and did not require additional corrections.

A multispectral image capture on the 12 of April 2017 from Sentinel-2 were used to calculate both NDWI and MNDWI. McFeeters' NDWI (1996) takes advantage of the high reflectance of water in the green band, the low reflectance in the NIR and the high reflectance in NIR by soil and vegetation (Xu 2006, 3026) translating in the following equation (1):

NDWI = Green- NIR/ Green +NIR *equation (1)*

Xu argued that NDWI was unable to remove built up noise when applied in areas with these features, given them positive values as water.
He proposed an alteration in the index calculation (equation 2), which involved the substitution of the NIR band by a middle infrared band (MIR) that had a higher digital number than the green band, resulting in the attribution of negative numbers to build up land and the reduction of noise and therefore a better separation between water and non-water features (ibid. 3027).

MNDWI = Green-MIR/ Green+ MIR *equation (2)*

These indices have been largely used in several studies and have proved to be very useful in mapping and automatic extract surface water features (Du et al. 2016, Andrade 2019, Gautam et al. 2015, Szabo et al. 2016, Gil et al. 2019, Nair et al. 2016).

After calculations of the indices, a threshold of zero was used to separate water from non-water surfaces, with values equal or above zero representing water features and negative the non-water ones. After the extraction of the water bodies identified in both indices its areas were calculated (Table 1).

To test the results, a small area located in the Serbian Banat region (Fig. 4) was chosen to act as a subset test area where 20 randomly disperse points were distributed (Fig. 5) and the values of the predicted locations evaluated through a confusion matrix (Table 2) using Google Earth and Planet imagery.
The selected area includes the villages of Sečanj, Neuzina, Sutjeska, Banatski Despotovac and Botoš and several water bodies, made of artificial ponds, for recreational fishing, and the Tamis River that crosses this area on its route to the Danube.

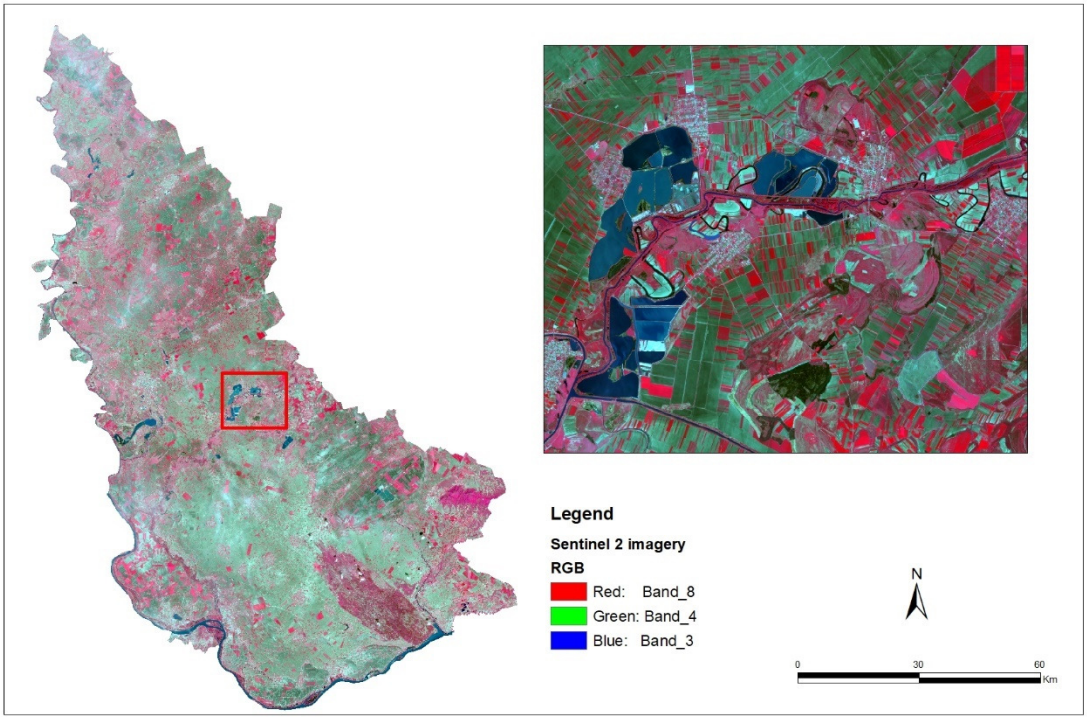

Figure 4: *Test area in Serbian Banat region*

Xu's contrast (*C*) value was also determined for both indices, through the calculation of the water bodies and background (non-water features) mean values. These were estimated by the extraction of values from points randomly distributed inside the water bodies boundaries and others distributed in the background.

A supervised classification using the maximum likelihood classifier was also performed using a false colour band composite, known as false colour infrared (FCC 8-4-3), obtained from Sentinel-2 imagery, as base map to attain the test samples required for the classification.

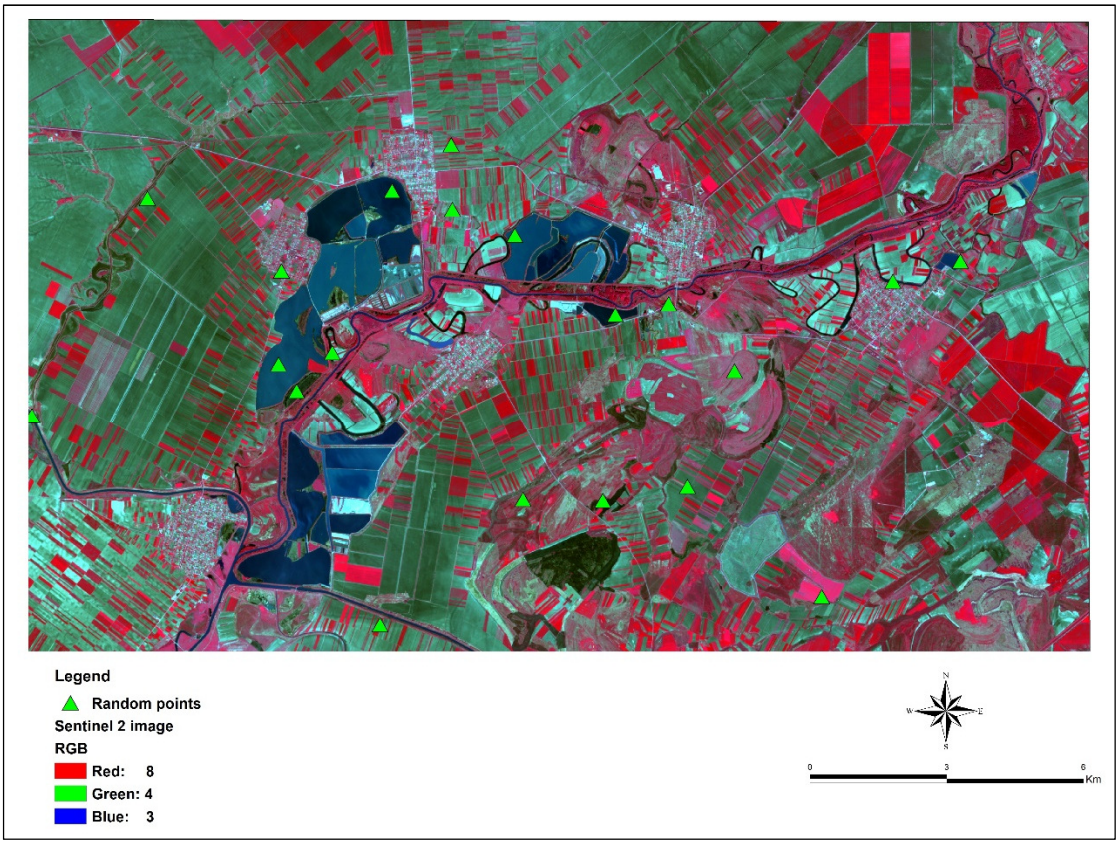

Figure 5: *Random point's location inside the test area.*

This band combination is commonly used in vegetation studies due to its ability to discern plants growth stage and health, however it can also be used in water studies, as these features stand out in black colour, or in blue if sediments are present in the water. The resulting open water bodies mapping were also extracted, the area occupied by them calculated, and the result of the classification tested using the subset area, and the values obtained added to the confusion matrix.

2.2. Sentinel-1 data

To perform two classifications using Sentinel-1 Synthetic Aperture Radar (SAR) data were downloaded from the Copernicus Open Access Hub (https://scihub.copernicus.eu/dhus/#/home), and while Sentinel-2 data didn't require further corrections, Sentinel-1 had to go through several steps before being used (Fig. 6).

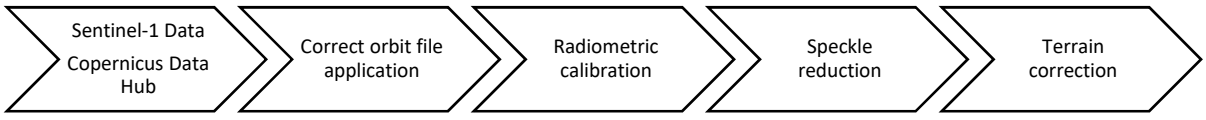

Figure 6: *Flowchart of the Sentinel-1 pre-processing.*

Level-1 ground range detected (GRD) dual polarized (VV and VH) data, from April 11 of 2017 were downloaded after which an orbit file correction was perform and a radiometric calibration was made. To reduce the speckle noise, the Lee spatial filter was applied, in a 5x5 window, and finally a terrain correction was performed, with the choice of the range doppler terrain correction. The resulting images were then subset to match the test area. A logarithmic scale conversion was applied to both bands to transform them in a decibel scale.

VV polarization data were chosen to perform the analyses as several studies had revealed that co-polarization achieved better results in water mapping than cross-polarization (Twele et al. 2016, Markert et al. 2020). All the procedures were made in the Sentinel Application Platform (SNAP) software.

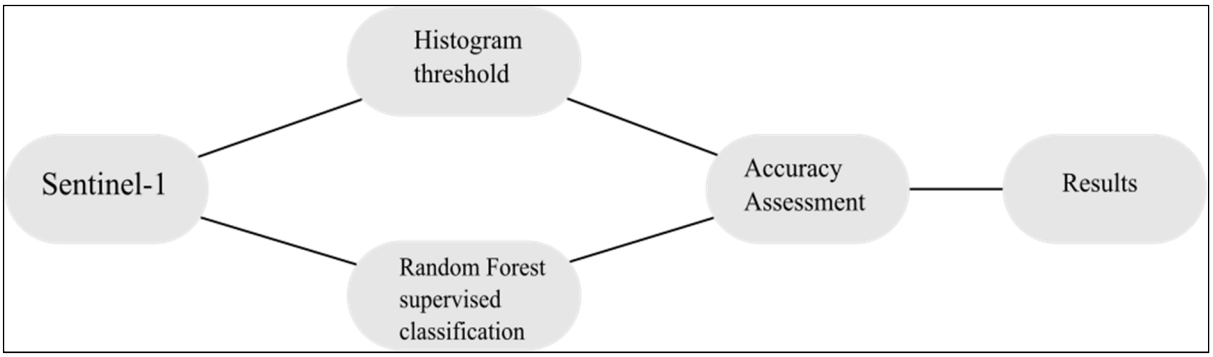

Figure 7: *Flowchart of methodological procedures for Sentinel-1 data.*

Using the SAR data two classifications were made. In the first, the common method of histogram threshold was used, in this approach "… all pixels with a backscatter coefficient lower than a specified threshold in an intensity image are mapped as water" (White et al. 2015, 7620). This is an easy and quick method to distinguish water from non-water features and widely used in studies (ibid., Liang, and Liu 2020, Westerhoff et al. 2013, Santoro et al. 2013, Schumann et al. 2010).

After analysing the intensity unimodal histogram (Fig. 8) and performing some tests with different thresholds, the value of -18 was chosen for the separation.

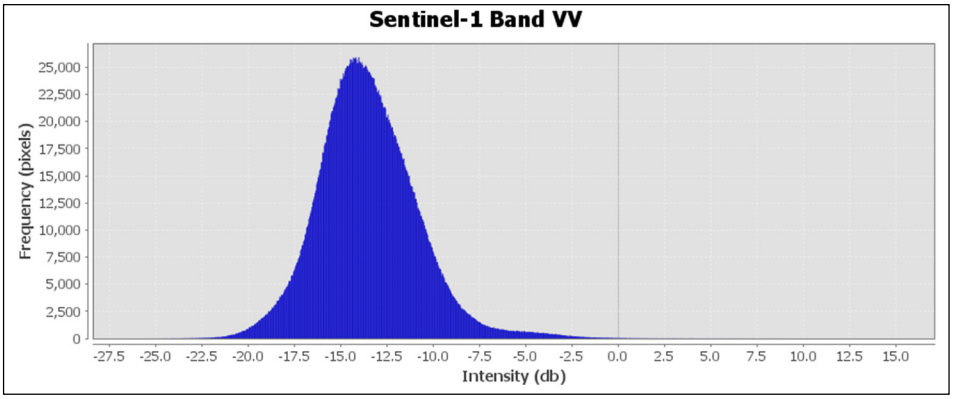

Figure 8: *Sentinel-1 Intensity histogram (11/04/2017)*

The second method to open water mapping involved a random forest (RF) supervised classification. This approach is also widely used in remote sensing data, particularly common in land cover studies (Niculescu et al. 2020, Gupta et al. 2015, Jhonnerie et al. 2015).

The open water bodies identified by both methods using SAR data were extracted, their areas calculated, and the results evaluated following the procedure applied to the approaches above mentioned, used in optical imagery, that involved testing the predicted location for 20 random points in the test area, and the construction of a confusion matrix.

3. RESULTS

NDVI water bodies mean value reached 0.41 and a standard deviation of 0.08, and the non-water features a mean value of -0.37 and a standard deviation of 0.17. MNDWI water bodies mean was 0.75 and the standard deviation 0.13, while non-water features mean was similar to NDWI but with a smaller standard deviation (Mean=-0.37, STD = 0.07). Using the resulting values of the means to calculate Xu's Contrast (2006), NDWI achieved the value of 0.78 and MNDWI 1.12.

As evident in Table 1 results, the water bodies area for NDWI was 17.42 Km^2, for MNDWI 17.70 Km^2, for the Maximum Likelihood (ML) classification 17.55 Km^2, for the SAR intensity threshold of -18 was 12.99 Km^2 and finally for the Random Forest (RF) classification 11.69 Km^2.

Table 1: *Water bodies areas*

Methodology	Area (Km^2)
NDWI	17.42
MNDWI	17.70
ML classification	17.55
SAR threshold classification	12.99
SAR Random Forest classification	11.69

Analysing the results of the confusion table (Table 2), NDWI achieved 85% overall accuracy and a Kappa coefficient of 0.71. It also got a lower value (zero) in the error of omission and 0.27 in the commission error. The producer's accuracy was the highest (=1) and the user's value was 0.73. MNDWI overall accuracy was 90% and its Kappa coefficient 0.79. Both errors of omission and commission reached the value of 0.13 and in the producer's and user's accuracy 0.88.

Maximum Likelihood (ML) classification obtain 95% overall accuracy and 0.89 in the Kappa coefficient calculation. Its error of omission and producer's accuracy was similar to MNDWI, but its commission error was lower (= 0) and the user's accuracy higher (=1). Both SAR classifications achieved the same results, with 75% overall accuracy and 0.42 in the Kappa coefficient.

Table 2: *Confusion matrix*

	Overall accuracy	Kappa coefficient	Error of omission (water)	Error of commission (water)	Producer's accuracy	User's accuracy
NDWI	85%	0.71	0	0.27	1.00	0.73
MNDWI	90%	0.79	0.13	0.13	0.88	0.88
ML classification	95%	0.89	0.13	0	0.88	1.00
SAR threshold	75%	0.42	0.63	0	0.38	1.00
SAR Random Forest	75%	0.42	0.63	0	0.38	1.00

4. DISCUSSION

The MNDWI obtained a better result than NDWI, with an accuracy of 90% and a 0.79 in Kappa coefficient. The resulting image from this index showed a darker tone than NDWI (Fig. 9), demonstrating a clearer separation between water and non-water elements as described by Xu's work (2006). Although, the area identified as water bodies was slightly bigger (17.70 km^2) than the one present in the NDWI result (17.42 Km^2), this is related to MNDWI spatial resolution (20 m) that was higher than the 10 m of NDWI.

MNDWI could probably achieve an even better result if a pan-sharpening of the SWIR band was done before the calculation of the index, as showed by Du and his colleagues (2016). The substitution of the NIR band by the SWIR, also led to an increase of the water bodies mean value, that is higher in the MNDWI, and although the background mean value was similar in both indices (-0.37) the bigger MNDWI water mean led to a higher contrast (*C*) value (1.12).

Although in Xu's work, NDWI non-water mean value presented a positive value, demonstrating the presence of built-up land as noise, in the test area the non-water mean achieved a negative mean, similar to MNDWI, indicating a noise reduction in both indices. Yet, looking at other areas of Serbian Banat (Fig. 10) this apparent NDWI noise reduction is not present in the whole region, and that MNDWI performed better reducing more built-up areas in comparison to NDWI.

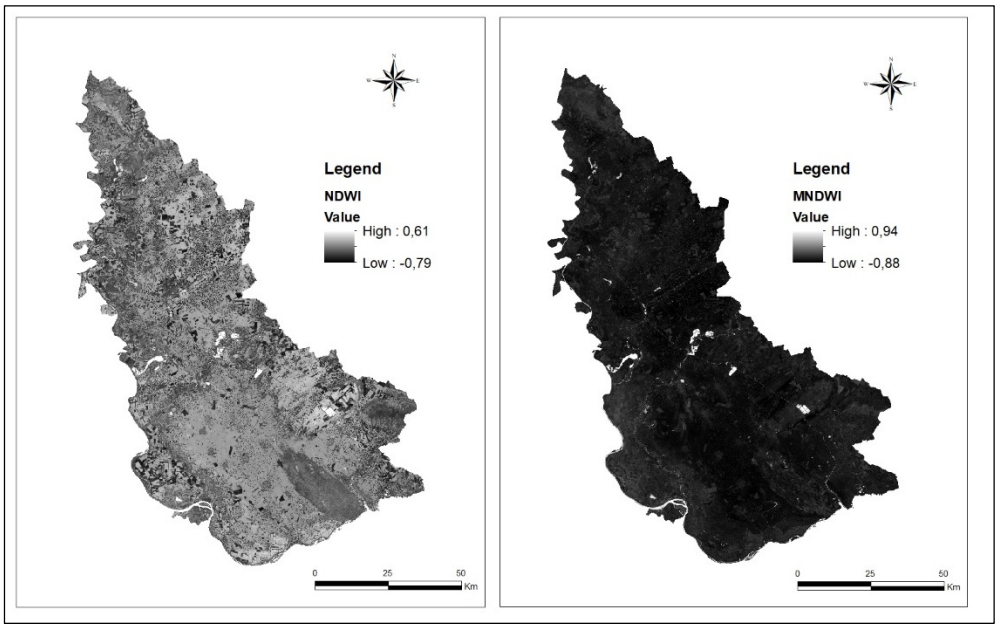

Figure 9: *NDWI and MDWI resulting imagery*

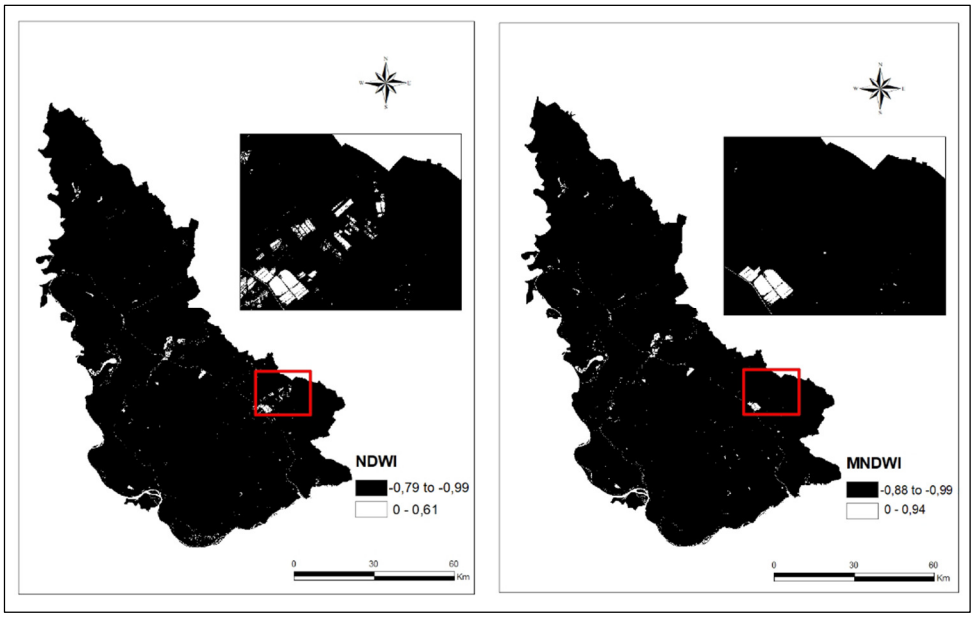

Figure 10: *NDWI and MNDWI built-up areas comparison*

The maximum likelihood classification obtained the higher values in the overall accuracy and Kappa statistics, 95% and 0.89 respectively, this way achieving the best performance result of all five methods tested.

Looking at the water bodies extracted from the several methods tested, differences in the areas can be seen, related to the correct identification of these features and the noise reduction (Fig.11-13).

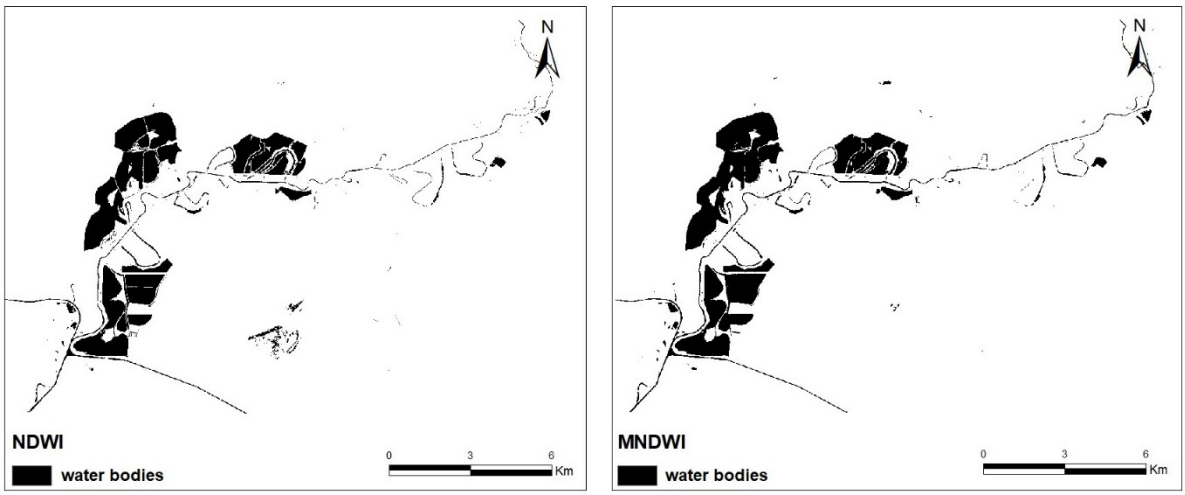

Figure 11: *NDWI and MNDWI waterbodies identification*

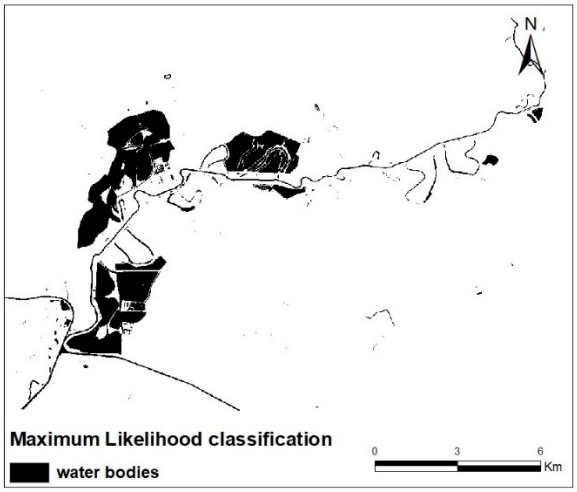

Figure 12: *Maximum likelihood water bodies identification*

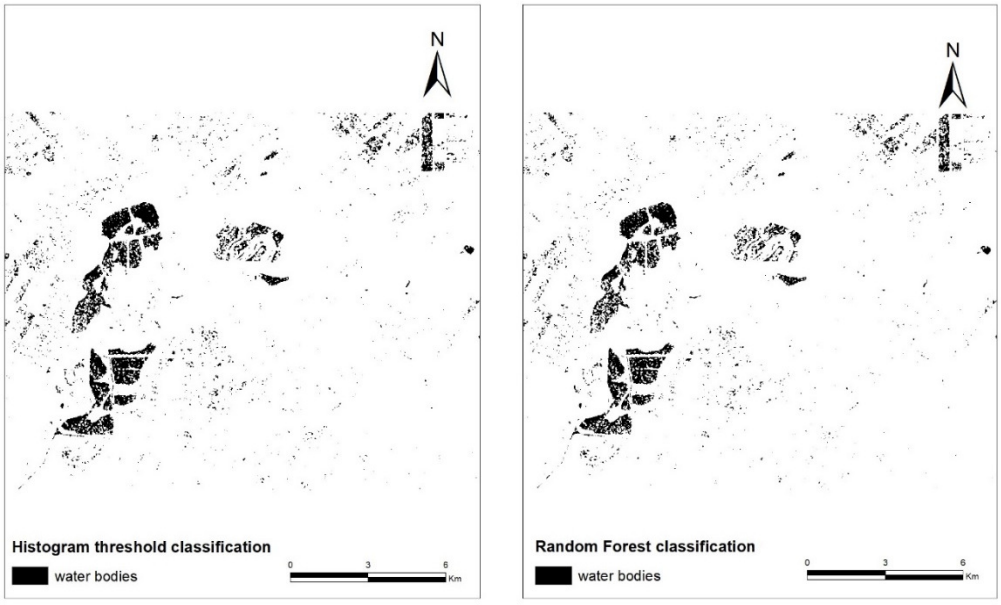

Figure 13: *Histogram threshold classification (left) and Random Forest classification (right)*

Both SAR classifications achieved the same values in the confusion matrix and a visual inspection of the resulting images showed a remarkable resemblance. These methods represent the lowest accuracy in the water mapping process by failing to detect most of the Tamis River course, probably by reason of the small width of the river in this area, and the presence of mixed pixels with values similar to the background features. Furthermore, values between -15 and -16 can be found in the river pixels, but also in some of the surroundings, probably due to an increase of moisture. This sensitivity to moisture, and therefore to the dielectric conductivity as to the roughness of the surfaces, has probably contributed to the lack of a clear separation of water/land in the histogram taken into consideration that April is a rainy month.

The problems around the delimitation of smaller rivers have already been discussed in the work of other researchers (Yang et al. 2014; Domeneghetti et al. 2014; Ogilvie et al. 2015). SAR sensitivity to roughness can also be seen in the pond's pixels discrimination. Looking at Fig.14, several pixels, with different backscatter values, can be found in the artificial lakes showing SAR sensitivity to surface differences. Overlay analysis using natural colour imagery were made to better understand variation in backscatter intensity values across these artificial shallow ponds. In the absence of ground truth data, it's hard to make a conclusion on whether these variation in intensity values are due to floating vegetation or plastic materials.

In the image it can also be seen that the dense canopy, located on both banks of the river and responsible for a strong volume scattering, could also have influenced the analysis.

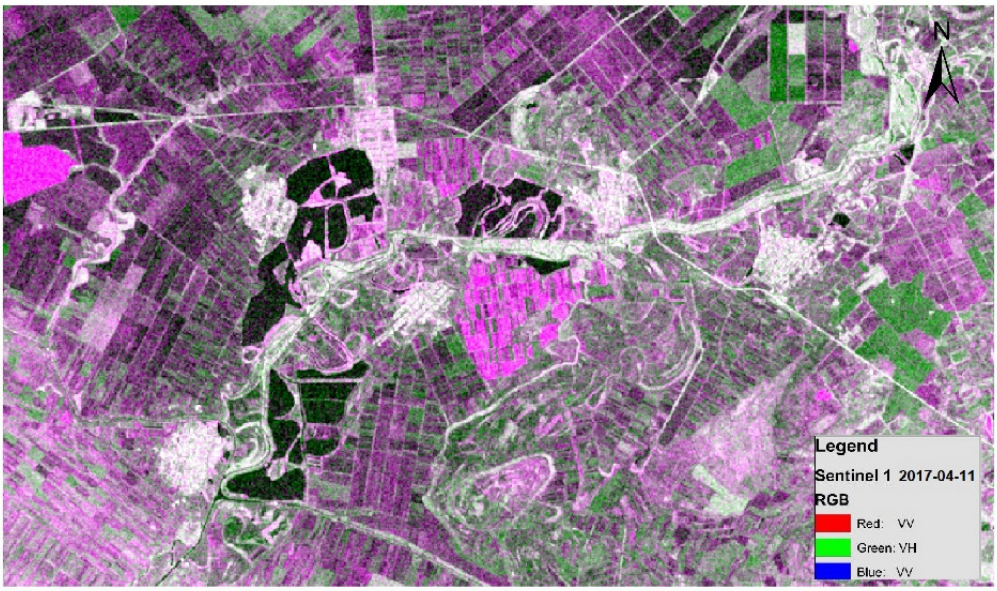

Figure 14: *Sentinel-1 image false colour composite.*

5. CONCLUSIONS

Using Sentinel-1 and 2 data, five different techniques were tested to verify their ability to successfully map water bodies for later extraction and analysis. Maximum likelihood supervised classification obtained the best results with an overall accuracy of 95% followed by MNDWI with 90% accuracy and a built-up noise reduction. All the three approaches using multispectral data successfully identified the river, however, in the event of a period of cloud cover or in the absence of sunlight, they will be incapable of doing so.

Although, the use of SAR can bring several advantages while mapping water and flooding events due to their ability to penetrate clouds, usually present during floods, in this comparative analysis their classifications come in last, as a consequence of the difficulty in mapping the Tamis River, probably

because of its small width in this area, and therefore to the reduced number of pixels. The presence of mixed pixels could have also contributed to this result as well as the volume scattering of dense canopy that surrounds the watercourse.

Since smaller rivers in the alluvial lowlands exhibit local flooding, as has been demonstrated in this area in the past, they should also be mapped and monitored. In this case other approaches should be used to map them more successfully, in the event of cloud cover.

M.E. acknowledges funding from the Irish Research Council, Government of Ireland Postgraduate Scholarship Scheme (Grant number GOIPG/2019/1271).

6. REFERENCES

Andrade, A. (2019). *Utilização dos índices NDWI e MNDWI na detecção de corpos hídricos em imagens Sentinel-2 na bacia hidrográfica do Rio Traipu–Alagoas*. Universidade Federal de Alagoas.

Domeneghetti, A., Tarpanelli, A., Brocca, L., Barbetta, S., Moramarco, T., Castellarin, A., Brath, A. (2014). The use of remote sensing-derived water surface data for hydraulic model calibration. *Remote Sens. Environ.*, 149, 130–141.

Du, Y., Zhang, Y., Ling, F., Wang, Q., Li, W., & Li, X. (2016). Water bodies' mapping from Sentinel-2 imagery with modified normalized difference water index at 10-m spatial resolution produced by sharpening the SWIR band. *Remote Sensing*, *8*(4), 354.

Gautam, V. K., Gaurav, P. K., Murugan, P., & Annadurai, M. J. A. P. (2015). Assessment of surface water Dynamicsin Bangalore using WRI, NDWI, MNDWI, supervised classification and KT transformation. *Aquatic Procedia*, *4*, 739-746.

Gil, A. P., Padovani, C. R., & Coelho, A. L. N. (2019). Comparação entre NDWI e MNDWI para o mapeamento de áreas inundadas no Pantanal do Taquari. In *Embrapa Pantanal-Artigo em anais de congresso (ALICE)*. In: SIMPÓSIO BRASILEIRO DE SENSORIAMENTO REMOTO, 19, 2019, Santos. São José dos Campos: INPE, 2019.

Gupta, S., Singh, D., Singh, K. P. and Kumar, S. (2015). An efficient use of random forest technique for SAR data classification. *2015 IEEE International Geoscience and Remote Sensing Symposium (IGARSS)*, 3286-3289.

Jhonnerie, R., Siregar, V. P., Nababan, B., Prasetyo, L. B., and Wouthuyzen, S. (2015). Random forest classification for mangrove land cover mapping using Landsat 5 TM and ALOS PALSAR imageries. *Procedia Environmental Sciences*, *24*, 215-221.

Liang, J., and Liu, D. (2020). A local thresholding approach to flood water delineation using Sentinel-1 SAR imagery. *ISPRS Journal of Photogrammetry and Remote Sensing*, *159*, 53-62.

Malinović-Milićević, S., Mihailović, D. T., Radovanović, M. M., and Drešković, N. (2018). Extreme precipitation indices in Vojvodina region (Serbia). *Journal of the Geographical Institute" Jovan Cvijic", SASA*, *68*(1), 1-15.

Markert, K. N., Markert, A. M., Mayer, T., Nauman, C., Haag, A., Poortinga, A., Bhandari, B., Thwal, N., Kunlamai, T., Chishtie,F., Kwant, M., Phongsapan, K., Clinton, N., Towashiraporn, P., and Saah, D. (2020). Comparing sentinel-1 surface water mapping algorithms and radiometric terrain correction processing in Southeast Asia utilizing google earth engine. *Remote Sensing*, *12*(15), 2469.

Mcfeeters, S.K., 1996, The use of normalized difference water index (NDWI) in the delineation of open water features. International Journal of Remote Sensing, 17, p. 1425–1432.

Nair, P. K., and Babu, D. S. (2016). Spatial Shrinkage of Vembanad Lake, South West India during 1973-2015 using NDWI and MNDWI. *International Journal of Science and Research*, *5*(7), 319-7064.

Niculescu, S., Billey, A. and Talab Ou Ali, H. (2018). Random Forest Classification using Sentinel-1 and Sentinel-2 series for vegetation monitoring in the Pays de Brest (France). *Remote Sensing for Agriculture, Ecosystems, and Hydrology XX* (Vol. 10783, p. 1078305). International Society for Optics and Photonics.

Ogilvie, A., Belaud, G., Delenne, C., Bailly, J.-S., Bader, J.-C., Oleksiak, A., Ferry, L., and Martin, D. (2015). Decadal monitoring of the Niger Inner Delta flood dynamics using MODIS optical data. *J. Hydrol.* 523, 368–383.

Pavlović, P., Kostić, N., Karadžić, B., and Mitrović, M. (2017). *The soils of Serbia*. Springer Netherlands. 225pp.

Santoro, M. Wegmuller, U. Lamarche, C. Bontemps, S. Transon, J. Arino, O. (2015). Strengths and weaknesses of multi-year Envisat ASAR backscatter measurements to map permanent open water bodies at global scale. *Remote Sens. Environ*. 171, 185–201

Szabo, S., Gácsi, Z., and Balazs, B. (2016). Specific features of NDVI, NDWI and MNDWI as reflected in land cover categories. *Landscape & Environment*, *10*(3-4), 194-202.

Schumann, G., Baldassarre, G.D., Alsdorf, D. and Bates, P.D. (2010). Near real-time flood wave approximation on large rivers from space: Application to the River Po, Italy. *Water Resour. Res. 46*, 1–8.

Twele, A. Cao, W. Plank, S. and Martinis, S. (2016). Sentinel-1-based flood mapping: a fully automated processing chain. *International Journal of Remote Sensing,* 37, 2990–3004.

Westerhoff, R., Kleuskens, M.P.H., Winsemius, H.C., Huizinga, H.J., Brakenridge, G., and Bishop, C. (2013). Automated global water mapping based on wide-swath orbital synthetic-aperture radar. *Hydrol. Earth Syst. Sci.* 17, 651–663.

White, L., Brisco, B., Dabboor, M., Schmitt, A., and Pratt, A. (2015). A collection of SAR methodologies for monitoring wetlands. *Remote sensing*, *7*(6), 7615-7645.

Xu, H. (2006). Modification of Normalised Difference Water Index (NDWI) to Enhance Open Water Features in Remotely Sensed Imagery. *International Journal of Remote Sensing* 27, 14, 3025-3033.

Yang, K., Li, M., Liu, Y., Cheng, L., Duan, Y., and Zhou, M. (2014). River delineation from remotely sensed imagery using a multi-scale classification approach. *IEEE Journal of Selected Topics in Applied Earth Observations and Remote Sensing*, *7*(12), 4726-4737.